Advances in Science and Technology Research Journal

Advances in Science and Technology Research Journal, 2026, 20(7), 241–262
https://doi.org/10.12913/22998624/219349
ISSN 2299-8624, License CC-BY 4.0

Received: 2025.12.22
Accepted: 2026.05.15
Published: 2026.06.01

Influence of moulding sands on microstructural features, mechanical properties, and wear behaviour of AA2024 by CO_2 process

Kadapa Vijaya Bhaskar Reddy[1], Aruri Devaraju[2], Moyya Sandeep[3], P. Prakash[4], Mohammed Zubairuddin[5], Singuru Madhavarao[6], Shahid Tamboli[7]

[1] Department of Mechanical Engineering, Marri Laxman Reddy Institute of Technology and Management, Dundigal, Hyderabad 43, India
[2] Department of Mechanical Engineering, Kakatiya Institute of Technology & Science, Warangal, Telangana, 506015, India
[3] Department of Mechanical Engineering, MLR Institute of Technology, Hyderabad, Telangana, 500043, India
[4] Mohanbabu University (Formerly Sree Vidyanikethan Engineering College), Tirupati, Andhra Pradesh, 517102, India
[5] Department of Mechanical Engineering, Aditya University, Surampalem, Andhra Pradesh, 533437, India
[6] Sagi Rama Krishnam Raju Engineering College, Bhimavaram, Andhra Pradesh, 530204, India
[7] Symbiosis International University, Symbiosis Institute of Technology, Pune, 412115, India
* Corresponding author's e-mail: shahidt@sitpune.edu.in

ABSTRACT

The present study explored the feasibility of replacing conventional silica sand with industrial waste–based moulding materials—blast furnace slag and ferrochrome slag – in the CO_2 casting of AA2024 aluminium alloy. Alternative mould media have been shown in earlier research to improve cooling behaviour and lessen environmental impact; however, AA2024 alloy and its tribo-mechanical response have received little attention. The impact of these moulding sands on wear behaviour, surface finish, mechanical characteristics, and microstructural features was methodically assessed in this study. According to thermal analysis, ferrochrome slag produced refined grain structures (~75 µm) by promoting faster heat dissipation. As a result, silica sand castings exhibited the highest tensile strength due to their relatively balanced solidification and lower internal stress levels. In contrast, ferrochrome slag castings demonstrated superior microhardness and enhanced wear resistance. Due to the strong strain-hardening effect, blast furnace slag showed increased compressive strength. Slag-based moulds deliver competitive performance with enhanced durability under sliding conditions, as demonstrated by surface roughness and tribological evaluations. Overall, the results demonstrate that blast furnace and ferrochrome slags are technically feasible and sustainable substitutes for silica sand in the production of structurally sound AA2024 cast components.

Keywords: silica sand, blast furnace slag, ferro chrome slag, surface roughness, heat transfer rate.

INTRODUCTION

Casting remains one of the most economical and versatile manufacturing routes for producing complex metallic components, particularly aluminium alloys used in aerospace, automotive, and structural applications. Because of its accessibility, affordability, and suitable bonding properties, silica-sand moulding has historically predominated among casting techniques. However, overexploitation of natural silica sand from coastal areas and riverbeds has led to serious environmental issues, including long-term resource depletion, ecological imbalance, and land degradation. Large amounts of metallurgical waste, such as blast furnace and ferrochrome slag, have accumulated due to rapid industrialisation. Despite its promising thermal and refractory properties, a

large portion of this waste remains underutilised. Waste-derived moulding materials, such as fly ash, red mud, and biomass ash, have been the subject of recent studies that have identified advantages, including increased mechanical strength, reduced defects, and faster cooling rates. However, there are still few systematic, application-focused studies on the high-strength AA2024 alloy, and most focus on general aluminium alloys, such as A356 or AA6061. Finding sustainable moulding alternatives that can preserve or improve the performance of AA2024 is essential from both technological and environmental perspectives, given its extensive use in aircraft fittings, automotive components, gears, and load-bearing structures, where its exceptional strength-to-weight ratio and fatigue resistance are key [1].

Several recent studies emphasise the strong relationship between thermal behaviour of mould, solidification rate, and final mechanical properties of aluminium castings. According to research, mould materials with higher heat conductivity can improve hardness and wear resistance, decrease microporosity, and refine dendritic structures. Alternative mould media can improve structural integrity and dimensional stability, as evidenced by non-destructive testing and microstructural analyses in recent research. Nevertheless, the current literature reveals two significant gaps despite these advancements. First, studies that concurrently assess microstructure, mechanical strength, machinability, and tribological response under various moulding sands are scarce for AA2024. Second, rather than offering a comprehensive thermomechanical-tribological evaluation, most earlier works focus on mechanical or microstructural analysis separately. Furthermore, there are few studies comparing industrial slag-based moulding sands under controlled CO_2 curing conditions, where heat transfer mechanisms, binder chemistry, and particle size uniformity are essential factors. These drawbacks underscore the need for an extensive experimental setup that not only examines sustainability issues but also establishes quantitative relationships between mould composition, casting quality, and performance attributes [2].

Non-destructive testing (NDT) was employed as the methodology in a study conducted by Idris et al. [3] to determine the admissibility of AA5083 alloy castings. They have discussed the value of dye penetrant inspection, radiography, and ultrasonic inspection in detecting fatigue-strength compromising shrinkage and porosity that can lead to surface cracks. They noted that NDT is a vital quality-control tool that enables the detection of defects without destroying the part, thereby saving money and materials. Similarly, under the NDT, Narasimha Murthy et al. [4] compared the A356 alloy castings prepared in sand and granulated blast-furnace slag moulds. Their findings showed that the slag moulds enhanced microstructural integrity, reduced porosity, and hardened the material. A radiographic analysis revealed fewer internal defects in the slag castings, indicating that the mould can be an alternative to the traditional sand mould. Narasimha Murthy et al.[5] have also conducted a comparable study, examining the physical and chemical properties of blast furnace slag, ferrochrome slag, and high-silica sand in foundry operations. They demonstrated that the slag materials were more thermally conductive and refractorious and had a lower rate of expansion, which directly affected the rate of solidification, minimised casting defects, and enhanced dimensional accuracy. This again demonstrated the efficacy of other moulding media in producing sustainable, perfect castings. Kathick Srinivasan et al. [6] studied the use of biomass ash as a partial replacement for silica sand in aluminium casting. Their results showed that the ash from biomass reduced the need for natural sand and increased tensile strength and hardness through controlled cooling rates. The plan offered significant economic and environmental benefits, highlighting the value of waste materials in the casting recycling process. Tijani et al. [7] applied a combination of NDT and parameter modelling to determine the fatigue life of aluminium alloys. They were able to identify crack initiation and development with high accuracy using acoustic emission and ultrasonic tests, thereby enabling estimation of fatigue life with reasonable accuracy without destructive testing. The techniques are primarily used in aerospace and automotive applications, where fatigue performance is of great importance. In Bovas Herbert Bejaxhin et al. [8], defects and grain-boundary hardening in stressed Al6061 were measured by using NDT and SEM. They discovered that porosity and microcracks reduced grain boundaries, leading to premature failure. They employed a powerful strategy to correlate microstructural attributes and defect distribution by integrating SEM and NDT. Lastly, Patil et al. [9] explored the frequency response method as an NDT technique

in casting defects. Their research showed that it is sensitive to variations in stiffness and damping caused by unseen flaws. They provide a quick, cost-effective, and reliable supplement to conventional NDT for quality control.

Recent AA2024-focused studies highlight how controlling solidification and surface modification can markedly improve performance. Khan et al. [10] demonstrated that vibration-assisted dynamic solidification with conformal cooling transforms the microstructure from dendritic to more uniform non-dendritic features, reducing grain size and improving hardness and UTS in permanent-mould AA2024 castings. Wang et al. [11] reported that intensive melt shearing during casting effectively tailors the as-cast structure, producing finer second phases and improved mechanical properties after subsequent deformation and T4 treatment, confirming the strong "processing as-cast genetics properties" link in 2024 alloy. Complementarily, Rafi et al. [12] showed that friction stir processing with TiB_2 reinforcement enhances the hardness and dry-sliding wear resistance of AA2024 surface composites, highlighting the roles of a refined microstructure and stable tribo-layers.

An examination of the literature reveals that a limited number of studies have been published on the AA2024 alloy. Thus, the current paper focuses on AA2024, an Al-Cu-based alloy considered the 2nd strongest member of the aluminium family after the 7000 series. It is a highly heat-treatable alloy renowned for its excellent workability, fatigue resistance, and superior surface finish, coupled with high tensile and yield strengths, albeit with relatively low ductility. Due to these qualities, AA2024 is widely used in structural and high-stress components (from aeroplane fittings to missile parts, automotive components, and precision hardware) that require high strength. It is also widely used as an alternative material for connecting rods, gears, and flat plates. This paper aimed to explore the possibility of substituting traditional silica sand with blast furnace slag and ferrochrome slag in CO_2 moulding processes. To accomplish this, flat plate castings were made from three mould compositions: silica sand, blast furnace slag, and ferrochrome slag, all mixed with 94 parts sand and six parts sodium silicate binder. The moulds were hardened by passing CO_2 gas through vent holes at a rate of 15 L/min for 15 seconds. The castings obtained were studied with respect to heat transfer properties (as reflected in time-temperature profiles), microstructure, mechanical properties, and wear behaviour. This combined analysis will determine the suitability of blast furnace slag and ferrochrome slag as environmentally friendly, high-performance alternatives to silica sand for producing defect-free AA2024 castings.

The present study addressed the following research question: Can industrial waste-based moulding sands such as blast furnace slag and ferrochrome slag effectively replace conventional silica sand in CO_2 moulding of AA2024 alloy without compromising, and potentially enhancing, microstructural refinement, mechanical strength, surface finish, and wear resistance? This work is novel because it compares three moulding media (silica sand, blast furnace slag, and ferrochrome slag) holistically under the same binder ratios and controlled CO_2 curing conditions. A multi-dimensional performance evaluation is then conducted. This study uniquely combines heat transfer analysis using thermocouple-based temperature profiling, optical microstructural characterisation, hardness distribution, tensile and compressive behaviour, machining surface roughness, coefficient of friction, wear rate, and SEM-based wear morphology, in contrast to the previous studies that focus on single-property analysis or different alloy systems. Furthermore, the work bridges the gap between performance-oriented casting optimisation and sustainability-driven material substitution by directly establishing correlations between the tribomechanical behaviour resulting from thermal-conductivity-induced grain refinement. By using this combined approach, the study offers valuable insights for foundries seeking to balance high-performance aluminium alloy production with environmental consciousness, as well as suggesting environmentally friendly moulding alternatives.

EXPERIMENTAL PROCEDURE

Materials

The material used in the current study is aluminium alloy AA2024-T351. The alloy is supplied in extruded rod form, which is cut into smaller sizes to ease casting. Optical Emission Spectroscopy (OES) was used in this research to determine the chemical composition of the aluminium alloy, using a Foundry-Master Pro

spectrometer. To be precise, the analysis was done using standard calibration procedures. The instrument had a measuring accuracy of 0.01 wt.% for the major alloying elements (Cu, Mg, and Si) and 0.005 wt.% for the trace elements. Table 1 shows the detailed results.

Moulding sand preparation

Silica sand comprises approximately 96% pure silica grains and 4% impurities. In this case, the silica sand was procured in Chirala, Andhra Pradesh. It was well sieved to remove foreign materials and dust, and then preheated to 300 °C for 3 hours to remove moisture before casting. The blast furnace slag, a by-product of the steel manufacturing process, was purchased at the Vizag Steel Plant through a contractor specialising in cement production. The slag was purified by sieving to remove impurities and subsequently preheated to 300 °C over a 3-hour period. After drying, the material was again sieved using mesh sizes of 70 to 20, and particles with a 30-mesh size were cast. Ferrochrome slag, a by-product of the ferrochrome manufacturing industry, was collected at Sarada Ferro Alloys in Visakhapatnam. The slag was in pellet form and crushed in two stages. To begin, the pellets were reduced to smaller particle sizes using a jaw crusher and then sieved to obtain ASTM 30-size particles. The rest of the oversized showed were once more minimised through a roll crusher and re-sieved. The subsequent ASTM 30-size slag was cast. For the three moulding materials, the sand-to-sodium silicate ratios were kept at 94:6. It was mixed by hand in trays, and each mould cavity was filled with an estimated 14 kg of ready-moulding sand. The preparation was uniform to give uniformity in all castings. Following initial binder optimisation trials in the 4–8% weight range, this proportion was determined. After CO_2 curing, 6 weight percent sodium silicate offered the best compressive strength, sufficient permeability, and acceptable collapsibility. While higher binder contents decreased venting capacity and increased the risk of gas porosity, lower binder contents resulted in weaker moulds that were more likely to erode. All materials were sieved to ASTM 30 mesh and uniformly preheated to reduce compositional bias among silica sand, blast furnace slag, and ferrochrome slag. As a result, mechanical stability and uniform curing behaviour across various particle chemistries were guaranteed by the chosen ratio. After crushing and sieving, the slag had an average particle size of approximately 106 µm, with a range of 75-150 µm. Standard sieve analysis was used to verify particle size distribution, ensuring uniformity in the moulding mixture. This range of sizes was chosen, because it offers the best mould strength, permeability, and surface finish. The chemical properties of the moulding materials from the slag were studied using Optical Emission Spectroscopy (OES), and the data, summarised in Tables 2 and 3, were used to determine the proportions of the main alloying components and trace elements.

Casting process

Pattern making

For this study, a wooden replica of the final casting was created using the pattern as a guide. Wood was chosen because it was

Table 1. Chemical composition of AA2024

Element	Mg	Cu	Cr	Fe	Si	Mn	Ti	Zn	Al
Wt.%	1.3	4.1	0.1	0.5	0.5	0.65	0.15	0.25	Bal

Table 2. Chemical composition of blast furnace slag

Composition	CaO	SiO_2	Al_2O_3	MgO	Fe_2O_3
Wt.%	44.1	34.2	12.4	7.8	1.6

Table 3. Chemical composition of blast furnace slag

Composition	SiO_2	Al_2O_3	MgO	CaO	Fe_2O_3	Cr_2O_3
Wt.%	33.2	19.4	27.0	3.1	9.2	1.7

inexpensive, readily available, lightweight, and easy to shape. During the casting process, a flat plate pattern measuring 12.2 × 5.1 × 2 cm – or roughly 125 cm³ – was utilised.

Mould preparation

In this study, a single-piece flat plate pattern was employed. The chosen moulding material, either ferrochrome slag, blast furnace slag, or silica sand, was packed around the pattern in the drag section of the mould for each casting. Until the drag section was filled, the mould material was added layer by layer and thoroughly compacted after each layer. Then, using a sprue and riser for metal flow, the cope mould was made in a similar manner. To aid in separation, facing sand was placed between the drag and cope. A vent rod was used to create vent holes throughout the mould after both sections were packed. The CO_2 gas used to harden the mould could pass through these holes. To ensure adequate hardening, CO_2 was injected into each vent for 15 seconds, with the gas flow rate maintained at 15 litres per minute (l/min).

Thermocouple setup

The current study aims to analyse the distribution of heat in different moulding sands used in the casting process. This was done through four-channel K-type digital thermometers connected to K-type thermocouples in an experimental setup. Eight thermocouples were positioned on one side of the mould cavity to monitor the temperature gradient between the centre and the outer wall. The thermocouples were placed in support tapes to maintain them after they were inserted five millimetres into the moulding sand. The heat flow characteristics of each type of moulding sand employed in the study can be thoroughly investigated.

Melting and pouring process

The primary objective of this research was to investigate how heat is distributed when using different moulding sands during the casting process. To achieve this, a four-channel K-type digital thermometer was prepared and equipped with K-type thermocouples. Eight thermocouples were attached to one side of the mould cavity. Note the temperature gradient by going to the outer wall and back. The thermocouples were inserted into the moulding sand to a depth of 5 mm and held in place with support tapes. Figure 3 illustrates the placement of these thermocouples, and their locations within the mould are explained in Table 4. This setup allows proper evaluation of heat-flow quality for each type of moulding sand used in the experiment. Once the mould was prepared, the cut AA2024 alloy pieces were washed and placed into a graphite crucible. The alloy was melted in a crucible furnace and heated to 700 °C, as shown in Figure 1a. The crucible was then placed in the

Table 4. Position of the thermocouple

Thermocouple No.	1	2	3	4	5	6	7	8
Position from the centre to the wall (mm)	0	5	10	15	25	35	45	55

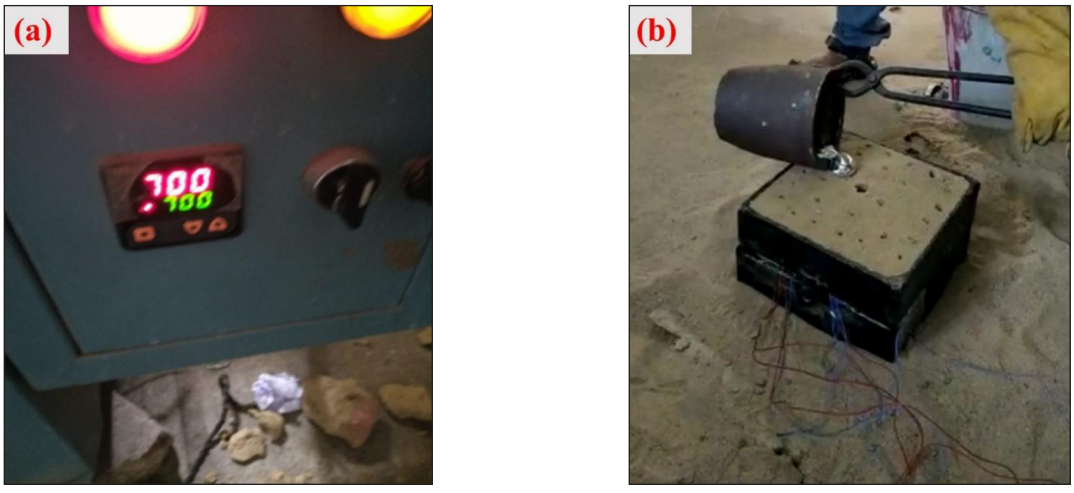

Figure 1. Photograph of (a) pouring temperature used, (b) pouring of molten metal

furnace with great caution using tongs. When the temperature was sufficiently high, the melted alloy was poured into the cast mould as indicated in Figure 1(b). The temperature was recorded at eight predetermined positions during post-pouring, with a 50-minute observation period to trackheat distribution. The casting was left to cool down to room temperature. The entire process was repeated with all types of moulds. When the casts had cooled, they were removed from the moulds by fettling, as shown in Figure 2.

Characterization of fabricated samples

An optical microscope (Model: Leica DM2700 M) was used for microstructural analysis. The cast components were hardened, and their hardness was determined using a 0.3 kg load applied for 15 seconds on a Zwick-Vickers hardness tester. The tests on tensile and compressive strength were conducted with a universal testing machine (Model: INSTRON-8801). The tensile specimens were made according to ASTM E8 standards, and their dimensions are shown in Figure 3. Compression test specimens were cylindrically shaped with H/D ratios of 0:1 and 1.5:1, as shown in Figure 4, and tested at a head speed of 1 mm/min under dry conditions. Wear testing was performed on a pin-on-disc (Model: TR-20LE) testing device to determine the coefficient of friction, mass loss, and wear rate of samples made from the three moulding sands. The tests were conducted with a constant load of 2 kg and two rotational speeds, 600 rpm and 780 rpm. The wear testing specimens had a length and diameter of 40 mm and 12 mm, respectively. Analysis of the worn surface morphology of the samples was performed using a scanning electron microscope (Model: HITACHI S-3000H) to determine the wear mechanism and surface degradation features.

Figure 2. Image of the cast component

Statistical analysis

To ensure the reliability of the experimental results, statistical analysis was performed for hardness, tensile strength, surface roughness, and wear rate data. Each test was repeated three times under identical conditions, and the mean and standard deviation were calculated. A one-way analysis of variance (ANOVA) was conducted at a 95% confidence level ($p < 0.05$) to evaluate the statistical significance of differences among silica sand, blast furnace slag, and ferrochrome slag castings. The obtained p-values confirmed that the variations in mechanical and tribological properties were statistically significant. Error bars representing standard deviation have been incorporated in the relevant graphs to improve data transparency.

RESULTS AND DISCUSSION

Density

Density measurements are a very informative tool for assessing the level of microporosity in castings produced with different mould materials. The cast of ferrochrome slag mould was

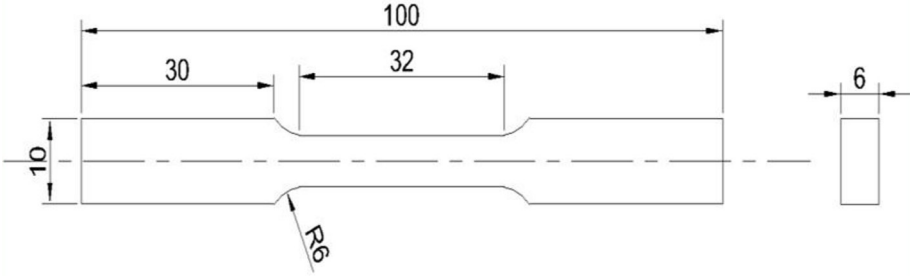

Figure 3. Dimensions of tensile test specimen

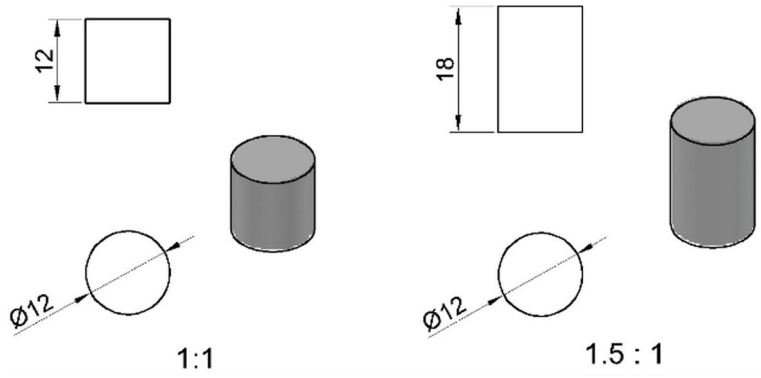

Figure 4. Dimensions of compression test specimen

the densest (2.74 g/cm³), which is very close to the theoretical density of AA2024 (2.78 g/cm³). In this way, the microporosity was reduced, and solidification occurred. In comparison, the blast furnace slag mould density was slightly lower (2.71 g/cm³), indicating that it was somewhat microporous due to slower cooling and deterioration of heat transfer. The density of the silica sand mould was the lowest (2.68 g/cm³), indicating greater microporosity and increasing the likelihood of gas trapping or shrinkage pores. These results agree with the mechanical and wear data, in which the ferrochrome slag castings, which were denser and had fewer defects, were stronger and exhibited greater wear resistance than silica sand castings [13]. In this way, the density value is an excellent parameter for estimating microporosity, without the need for high-tech radiographic or ultrasonic tests, underscoring the importance of mould material selection in determining the overall quality and integrity of cast items.

The observed density variation among the three moulding sands directly reflects the influence of cooling rate and gas permeability on internal defect formation. Comparatively higher thermal conductivity of ferrochrome slag enabled rapid solidification, reducing entrapped gases and shrinkage cavities and producing castings closer to theoretical density [14]. On the other hand, the moderate cooling behaviour of silica sand increased microporosity by permitting limited gas escape. Because of localised pore clustering and slower heat extraction, blast furnace slag exhibited intermediate behaviour, albeit with a slightly lower density. These results highlight that density measurement is a good indirect indicator of casting integrity, especially when sophisticated NDT facilities are not available, and that mould thermal response controls metallurgical soundness.

Microstructure

Figure 5 illustrates the optical micrographs of AA2024 alloy castings with the aid of silica sand, blast furnace slag, and ferrochrome slag as a moulding material using the CO_2 casting. The ferrochrome slags from the three moulds were found to have the best grain structure, the best thermal conductivity, and the fastest cooling rate, as shown by the time-temperature curves. The microstructures exhibited dendritic growth, consisting of a blend of coarse and fine grains, with epitaxial dendritic α-Al and 0-phase. These dendritic characteristics are attributed to the effect of magnesium and other alloying elements in the eutectic phases, together with solidification dynamics. Figures 5a and 5b show a significant decrease in the distance between the dendritic arms with increased cooling rate.

Figure 5b demonstrates that the distance between the dendritic arms is larger when the blast furnace slag mould is cooled more slowly. This confirms a critical role of the cooling rate on dendritic morphology and grain refinement [15]. The sizes of the grains were observed to range between 75.1 µm and 115.5 µm, with the smallest size recorded in ferrochrome slag (75.1 ± 2 µm), coarsest in the blast furnace slag (115.5 ± 5 µm), and in between in silica sand (101.4 ± 3 µm), as shown in Table 5.

The microstructural refinement of ferrochrome slag castings is a clear example of the influence on the speed of dendritic development. Besides reducing solute segregation, a high solidification rate promoted consistent α-Al dendritic structures and a finer spacing of dendritic arms (SDAS). The blast furnace slag moulds, on the other hand, generated broader SDAS, coarser grains, and localised segregation due to slower

heat dissipation. Silica sand castings exhibited an intermediate response, indicating moderate cooling properties. These differences significantly affect the mechanical and corrosion performance of the alloy with respect to grain size. According to the Hall-Petch effect, finer grains enhance strength, ductility, and corrosion resistance by reducing microgalvanic activity and increasing dislocation resistance [16].

Microstructural refinement observed in ferrochrome slag castings highlights the critical role of heat transfer efficiency in controlling dendritic evolution and secondary dendrite arm spacing (SDAS). In addition to promoting uniform α-Al matrix formation with finely distributed eutectic constituents, faster cooling suppressed solute segregation. On the other hand, delayed solidification can lead to the formation of coarse dendrites in blast furnace slag, which can negatively affect hardness and crack resistance. The moderate refinement of silica sand confirmed its traditional use, but it also showed little room for optimization. Grain size reduction confirms that mould composition significantly affects metallurgical homogeneity and subsequent performance characteristics. It also stabilises wear behaviour by reducing localised stress concentrations and improving strength through Hall-Petch strengthening [17].

The presence of ferrochrome slag indirectly influences corrosion and oxidation resistance by refining the microstructure and stabilising oxide films. Faster cooling produces finer grains and reduced porosity, which minimises microgalvanic cells and crack-initiation sites. Furthermore, chromium-rich slag components may promote the formation of more stable and adherent surface oxide layers, thereby enhancing resistance to environmental deterioration. The refined microstructure suggests improved corrosion tolerance, despite the lack of specific electrochemical testing.

A noticeable variation in grain size distribution was observed among the moulding materials. Ferrochrome slag castings exhibited the finest and most uniform grains due to faster heat dissipation and higher thermal conductivity. In contrast, blast furnace slag produced relatively coarse dendritic structures due to slower cooling.

Table 5. Grain size of all the casted components

Moulding material	Grain size
Silica sand	101.4 ± 3 µm
Blast furnace slag	115.5 ± 5µm
Ferrochrome slag	75.1 ± 2 µm

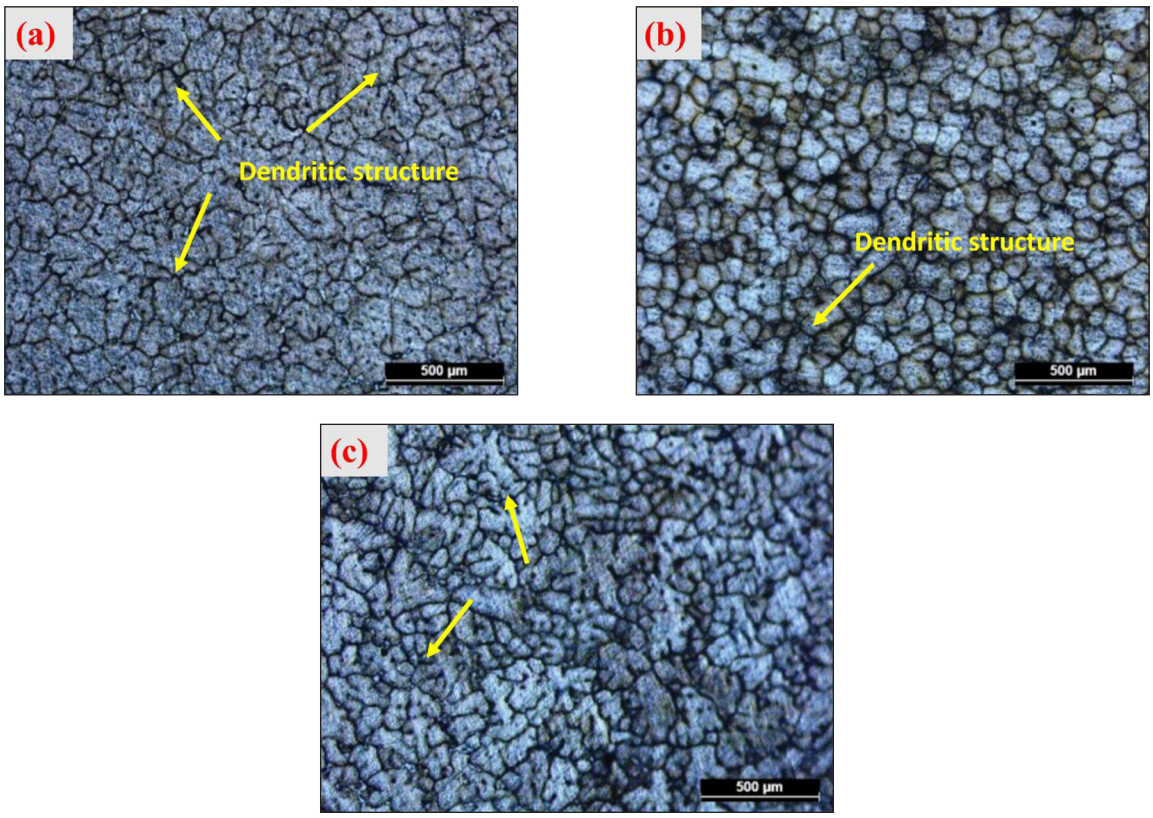

Figure 5. Optical micrographs of a flat plate: (a) silica sand, (b) blast furnace slag, (c) ferrochrome slag

Silica sand castings demonstrated intermediate grain sizes. These variations had a significant impact on the overall performance of AA2024 alloy; coarser grains improved ductility but decreased surface durability, while finer grains improved hardness, tensile strength, and wear resistance through Hall–Petch strengthening [18]. As a result, the distribution of grain sizes is essential for determining the tribological stability and mechanical reliability of cast components.

Heat transfer analysis

A time-temperature curve is drawn to determine the flow of heat through the sand particles in moulding when molten metal is added to the mould, with temperature on the y-axis and time on the x-axis. Degrees Celsius and minutes are used to record the temperature and time, respectively. The paper analyses the heat transfer rate in three moulding sand castings based on temperature distribution graphs. Each moulding sand has thermocouples at 8 locations: 0 mm (centre), 5 mm (near the cavity wall), 10 mm, 15 mm, 25 mm, 35 mm, 45 mm, and 55 mm. In this way, three graphs on distribution are created. All the samples were heated to 700 °C, and the heat distribution was monitored for 50 minutes. Heat flow was measured on one side of the casting within the mould cavity. Figure 6 illustrates the time profiles of heat transfer for all the moulds. The result is a pronounced decrease in temperature at the centre over time [19]. The other seven posts depict varying levels of heat transfer. The larger the distance from the centre, the smaller the fluctuation. Another interesting feature is that the temperature decreases significantly at both the centre and 5 mm points, as they are in direct contact with the molten metal, a significant source of heat loss. The temperature first increases at 10 mm and 15 mm, then it continuously decreases as heat is dispersed throughout the mould. Other jobs have low levels of fluctuation. Figure 8c indicates that the ferrochrome slag has a higher cooling rate than silica sand and blast furnace slag. This is confirmed by a sharp decrease in temperature at the centre. The rapid heat dissipation is attributed to the high thermal conductivity of ferrochrome slag, which results in a smaller grain size, as observed in the microstructural analysis. Therefore, the most critical factor in heat dissipation is thermal conductivity, which explains why the results for ferrochrome slag are the best among the others. The thermal conductivity of the mould and its thermal

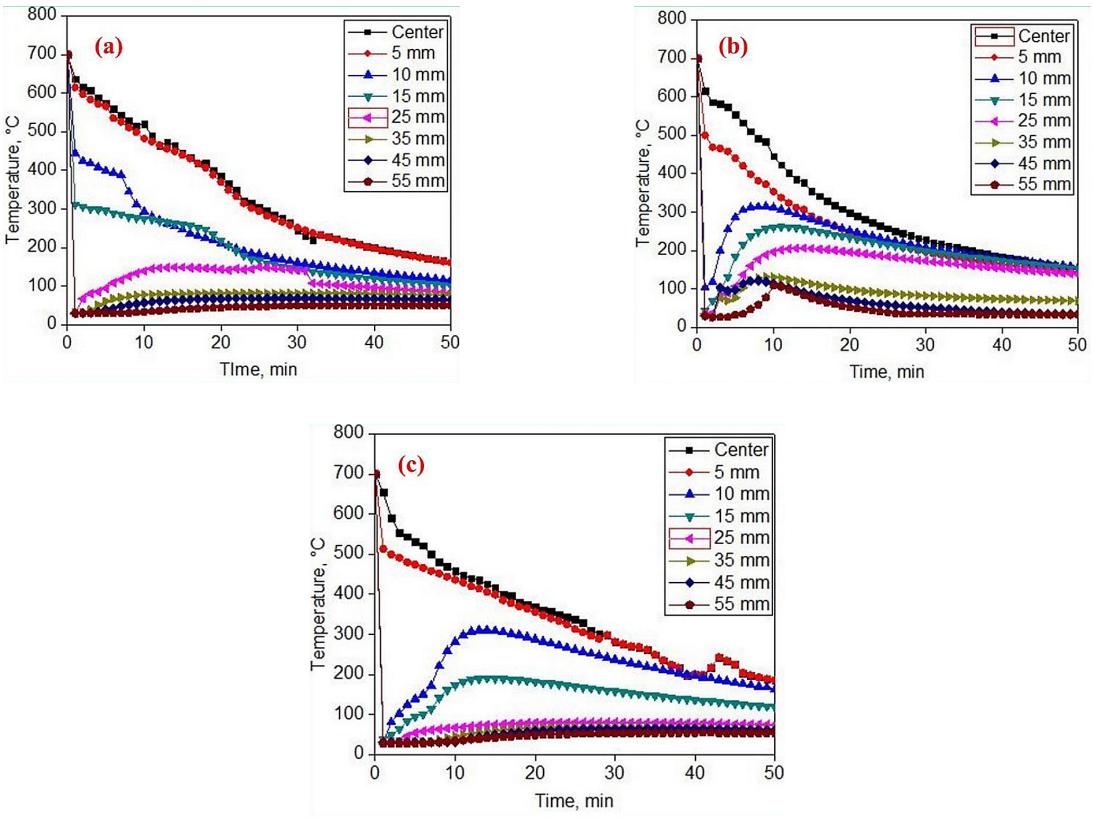

Figure 6. Time – temperature graph of a flat plate: (a) silica sand (b) blast furnace slag (c) ferro chrome slag

response, in relation to cooling behaviour, are evident in the heat transfer analysis. An increase in ferrochrome slag conductivity enabled a steeper temperature gradient, resulting in refined grains and increased hardness. The lower conductivity of the blast furnace slag, on the contrary, facilitated slower cooling and coarse dendrites. Silica sand exhibited average performance, as is the case in its traditional foundry practice. Local variations in solidification due to temperature differences between centres and walls also contributed to variations in the uniformity of grain and defects. In general, the findings indicate that interfacial heat transfer needs to be controlled, as fast homogeneous cooling decreases porosity and segregation, thereby increasing the structural integrity and mechanical behaviour of the castings.

The thermocouple-based temperature profiling provides quantitative evidence that interfacial heat dissipation varies significantly with mould chemistry and particle morphology. To produce refined grains and greater hardness, ferrochrome slag produced steeper thermal gradients, accelerating nucleation rates and shortening solidification times. Due to its lower conductivity, blast furnace slag exhibited delayed cooling, resulting in localised microsegregation and heterogeneous thermal zones. Heat flow in silica sand was balanced but less effective. These variations demonstrate that mould thermal diffusivity is a determining factor in selecting sustainable casting materials, as it not only shapes cooling curves but also directly affects microstructural homogeneity, porosity reduction, and mechanical reliability.

Microhardness analysis

Figure 7 illustrates the hardness distribution of the castings of the flat plates with the various moulding sands. The results of the microhardness tests suggest that the maximum hardness is achieved with ferrochrome slag at 153.5 HV, silica sand at 139.1 HV, and the lowest hardness is observed in blast furnace slag at 134.5 HV. This difference can mainly be attributed to the thinner grain structure formed in the ferrochrome slag mould, resulting from its higher cooling rate and thermal conductivity compared with those of the other sands. The flat plate part, cast on a one-piece pattern, has the most significant area of contact with the drag part of the mould, where heat is carried off most vigorously, especially at the bottom. This is attributed to the increased base wall, which encourages quicker cooling [2,20]. Conversely, the flat plate sides have fewer contacts with the mould, hence little heat transfer. Also, the top surface, which is in contact with the cope, is not entirely in contact with the moulding material; therefore, the amount of heat dissipated at the top is reduced. Although it is a partial contact, some amount of heat is conducted by surface conduction. Several factors besides grain refinement cause hardness variation. Although ferrochrome slag produced finer grains, which increased hardness through the Hall–Petch mechanism, strain hardening, differences in thermal conductivity among the mould materials, and redistribution of precipitates during solidification were all important factors [21]. An example was the blast furnace slag moulds, which yielded coarser grains that were less hard but stronger due to strain hardening. Comprehensively, hardness in the castings made of AA2024 is a conglomeration of the effect of grain size, the phase stability of the precipitate, strengthening of the solid solution, and hardening of the casting caused by deformation instead of grain refinement [22].

Defect content and microstructural refinement are closely related to the variations in hardness seen among the samples. Ferrochrome slag castings exhibited the highest hardness due to Hall-Petch strengthening, which is attributed to their fine-grain structure and reduced porosity. Conversely, silica sand castings exhibited intermediate hardness, while blast furnace slag castings showed the lowest hardness due to their coarse-grained structure and higher microporosity. Uneven cooling rates within the mould cavity are further indicated by local hardness variations between the drag and cope surfaces. All things considered, these findings indicate that hardness is a reliable predictor of cooling effectiveness and structural homogeneity, underscoring the importance of selecting mould materials with high thermal conductivity.

The hardness distribution trends correlate strongly with microstructural uniformity and defect density. Reduced porosity and refined grains improved the resistance of ferrochrome slag castings to plastic indentation by acting as dislocation barriers. Because coarser dendritic networks and uneven precipitation diminish lattice resistance, blast furnace slag samples have a comparatively lower hardness. Because of their moderate cooling behaviour, silica sand samples showed intermediate hardness. Different cooling

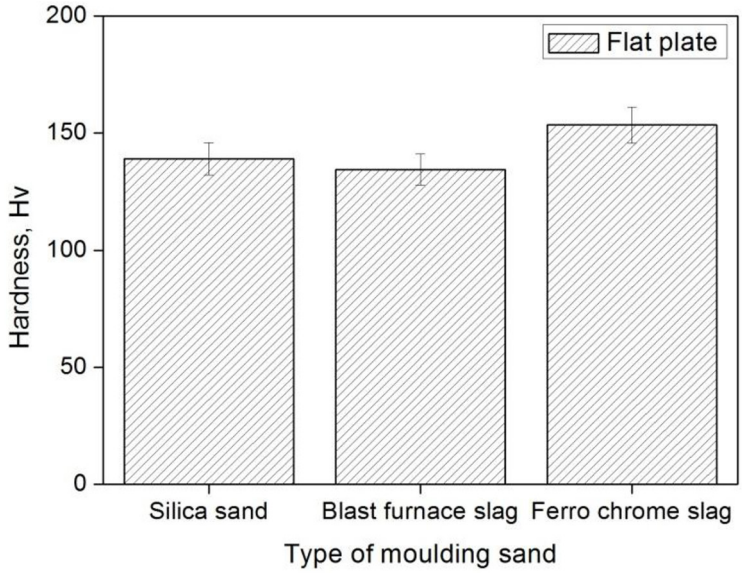

Figure 7. Microhardness survey of a flat plate

rates within the mould cavity are also indicated by localised hardness variations between the cope and drag surfaces. These results demonstrate that precipitate distribution, strain hardening, and microvoid concentration all affect hardness in addition to grain dependence.

Tensile strength analysis

An assessment of the tensile properties of the AA2024 alloy castings made using three moulding sands at room temperature is shown in Figure 8. The results indicate that the moulding sand significantly influences tensile performance. Silica sand castings had the highest ultimate tensile strength, followed by ferrochrome slag mould castings, and then blast furnace slag mould castings. The same was similar to the yield strength of 0.2%. It is interesting to observe that the elongation (percentage) was the least in ferrochrome slag and silica sand, and the greatest in blast furnace slag, which indicates an inverse linear relationship between ductility and tensile strength in this case. Microstructural studies confirm that the high tensile strength of ferrochrome slag castings is attributed to their smaller grain size and lower porosity [8]. The reduced tensile strength of the blast furnace slag mould, on the other hand, can be attributed to coarser grains and micropores. As the alloy is loaded, these pores concentrate stress, leading to cracks within the lattice. Neighbouring pores accelerate the propagation of a crack once it forms, leading to early failure. The existence and distribution of microstructural defects, therefore, significantly affect the mechanical integrity of cast components, and ferrochrome slag exhibits the most effective tensile properties.

The increased tensile strength observed in ferrochrome slag castings can be attributed to the refinement of grains and reduction of defects in the castings. Fine grains increase overall strength by delaying the initiation of cracks and acting as barriers to dislocation movement. Conversely, because these defects act as stress concentrators under applied loads, blast furnace slag castings with coarser grains and micropores showed lower tensile strength [23]. However, the traditional strength-ductility trade-off, in which larger grains improve plasticity, is reflected in their greater elongation. These findings demonstrate the superior suitability of ferrochrome slag moulds for structural components that require both high strength and reliability and support the strong correlation between microstructure and mechanical properties.

Tensile performance reflects the combined influence of grain refinement, porosity distribution, and intermetallic phase stability. Ferrochrome slag castings showed improved ultimate strength due to their finer grains and lower defect density, thereby delaying the onset of cracks. Because of its moderate ductility and balanced cooling, silica sand showed tensile values similar to those of other sands. Micropores acted as stress concentrators, accelerating fracture propagation, which is the primary reason blast furnace

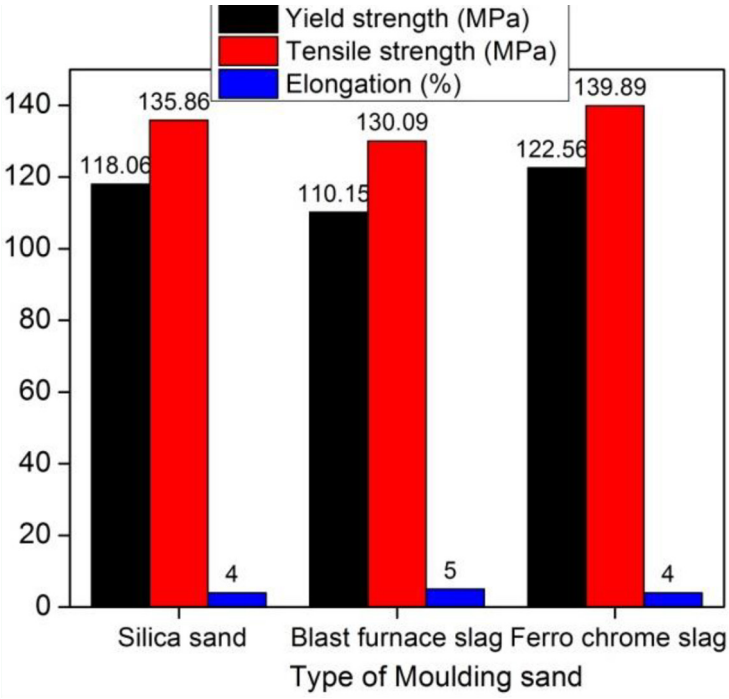

Figure 8. Tensile properties of a flat plate

slag samples had reduced tensile strength. The traditional strength–ductility trade-off is highlighted by the inverse relationship between elongation and strength seen in slag-based castings. These findings support the idea that microstructural integrity, rather than just hardness, controls tensile behaviour.

Compressive strength analysis

The compressive properties of the AA2024 alloy castings made with three different moulding sands were evaluated using the specimens with H/D ratios of 1:1 and 1.5:1. As shown in Figures 9 and 10, load-displacement curves were used to examine the impact of moulding sand on compressive strength. According to the results, ferrochrome slag moulds showed the lowest compressive strength, while castings from blast furnace slag moulds showed the highest across both H/D ratios. A greater load requirement was correlated with increasing displacement in both types of specimens. The actual stress-strain curves showed similar patterns. Additionally, the ferrochrome slag mould exhibited better ductility in the 1.5:1 configuration, whereas the blast furnace slag mould showed greater ductility in the 1:1 ratio. The slag component had the added advantage of enjoying the better strain hardening of the same when compressed, and this gave it high compressive strength despite its coarse-grain nature as compared to the ferrochrome slag casting that had a finer-grain structure [9]. This means that strain hardening is more important in establishing compressive behaviour than grain size alone. Its plastic-deforming nature is also illustrated by the greater resistance of blast furnace slag samples to compressive deformation; therefore, it is more applicable in load-bearing operations where compressive loads predominate. Besides grain refinement, strain hardening is also influential to the compressive strength of the castings. Ferrochrome slag (FCS) castings had improved hardness because of the creation of smaller grains, whereas blast furnace slag (BFS) castings exhibited higher compressive strength largely because of hardening on deformation. The higher density of dislocations during BFS casting also provided an advantage, increasing resistance to compressive loads. Consequently, although grain refinement has a larger effect on the balance of properties, both strain hardening and microstructural refinement contribute to the overall mechanical response.

Although it has a coarser grain structure, BFS moulds were more compressive, suggesting that, under compressive loading, strain hardening plays a more significant role than grain refinement. Larger grains allow greater plastic deformation, and the local work hardening increases resistance to compressive stress. On the other hand, FCS

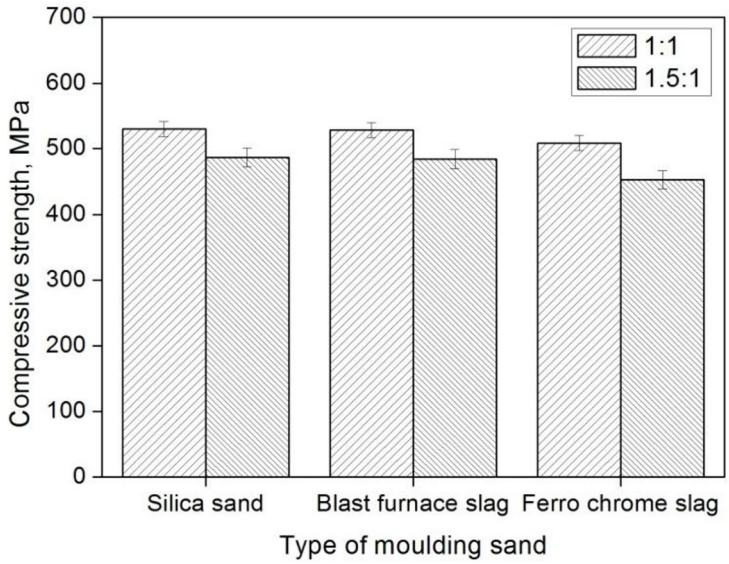

Figure 9. Compression strength of a flat plate

castings were less compressive, despite being stronger in tensile strength, because their fine-grained microstructure had a low strain-hardening capacity. This difference in mechanisms is essential; therefore, tensile and compressive behaviour are governed differently. The findings suggest that loading type is a factor to consider in selecting a mould: FCS is more efficient in a tension-based setting, whereas BFS is most efficient in a compression-based setting.

Unlike tensile behaviour, compressive strength is more sensitive to strain-hardening capability than to grain refinement. Because of their greater plastic deformation capacity and higher dislocation density, blast furnace slag castings demonstrated superior compressive resistance, enabling them to sustain higher compressive loads without catastrophic failure. Despite having finer grains, ferrochrome slag castings had a relatively lower compressive strength due to their limited ability to harden under continuous deformation. The behaviour of silica sand was characterised as intermediate. This distinction demonstrates that, since deformation mechanisms, not just microstructural refinement, govern compressive performance, mould selection should take the intended loading condition into account.

Surface roughness analysis

Surface roughness represents the texture of a component's surface and is quantified by measuring deviations from an ideal, smooth surface. The surface can be considered rough when these variations are significant, which may lead to increased wear, corrosion, and friction. A smooth surface, on the other hand, results in less wear, less friction, and a longer service life. Rough surfaces are

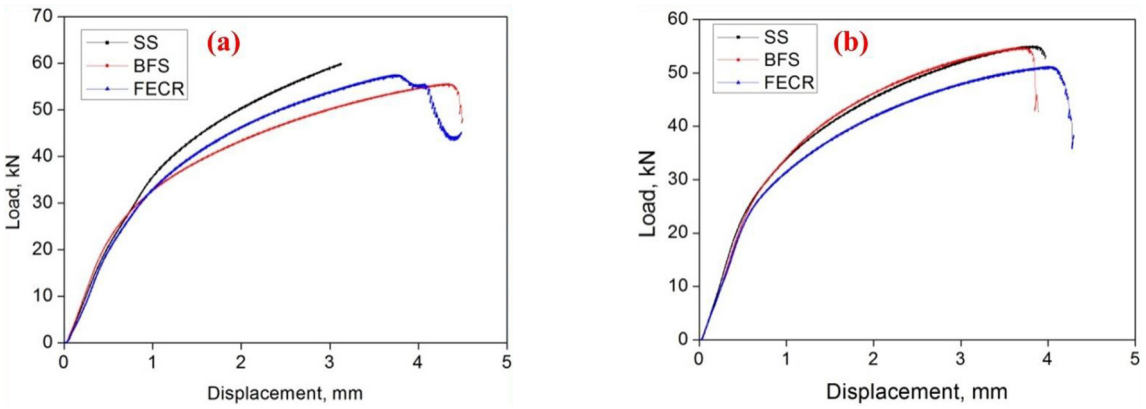

Figure 10. Stress vs strain graph of a flat plate: (a) silica sand, (b) blast furnace slag, (c) ferro chrome slag

more prone to wear and corrosion because they interact with the environment more forcefully. In this study, the cast components were made using ferrochrome slag, blast furnace slag, and silica sand as moulding materials, and then milled. A cutting speed of 1600 rpm, a depth of cut of 0.5 mm, and a feed rate of 0.1 m/s were among the machining parameters. To minimise friction, coolant was applied while each part was firmly clamped in a CNC milling machine. A Tally Surf device was used to measure the surface texture that developed during tool contact. The surface roughness profiles of the flat plate castings are shown in Figure 11. The blast furnace slag mould had the highest surface roughness (0.463 Ra), while silica sand had the lowest (0.415 Ra). Compared to blast furnace slag, ferrochrome slag had a marginally lower roughness (0.458 Ra). The softening of the AA2024 alloy at high cutting speeds, which enables the cutting tool to penetrate deeper and leave more noticeable surface indentations, is responsible for the increased roughness in the blast furnace slag sample [2]. Compared to the other moulds, this produces a rougher finish.

The difference in surface roughness of moulding materials is closely related to their thermal behaviour during solidification. Due to microstructural softening caused by high-speed machining, which promoted greater tool penetration and flaky chip formation, castings from blast-furnace slag exhibited the greatest roughness. Contrary to silica sand castings, silica sand castings provided smoother surfaces due to uniform solidification and heat transfer, thereby minimising tool-material interaction during machining. The middle level of roughness of ferrochrome slag castings was a trade-off between moderate machinability and high hardness. Overall, the results suggest that although slag-based moulds can provide positive mechanical strength enhancements, accurate optimisation of machining parameters is necessary to achieve surface finishes that meet functional requirements.

Surface finish variations reveal the interaction between microstructural hardness and machining dynamics. Higher roughness was observed in blast furnace slag castings due to unstable chip formation during high-speed milling and localised softening. Because balanced hardness reduced vibration effects and tool penetration depth, silica sand produced smoother surfaces. The trade-off between increased hardness and decreased machinability was evident in the moderate roughness of ferrochrome slag samples. According to these findings, mould-induced microstructural alterations affect post-processing quality, and to achieve the required surface integrity without sacrificing dimensional accuracy, slag-based castings require optimal machining parameters.

Coefficient of friction analysis

Figure 12 depicts the curve of the coefficient of friction (COF) of the flat plate components cast with various moulding sands at different slide distances of 2 and 33 cm rotating at 680 rpm and

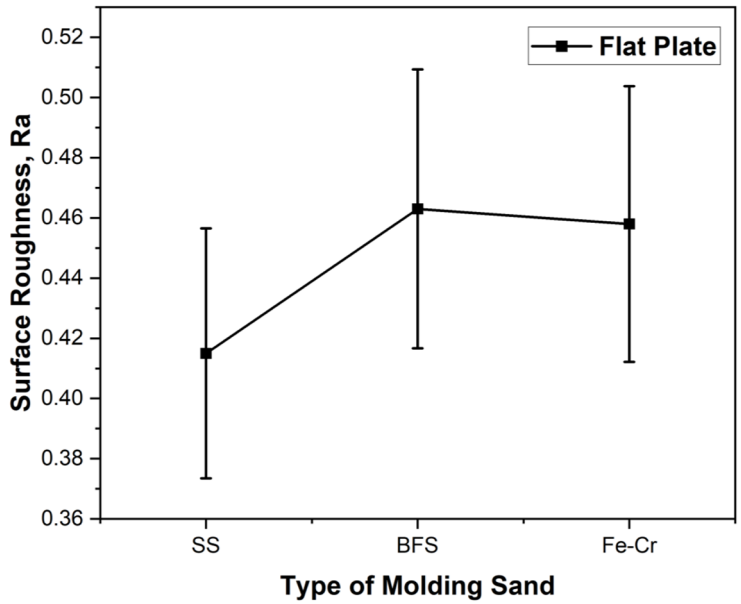

Figure 11. Surface roughness graph of a flat plate

780 rpm. On the basis of the data, COF typically decreases with the addition of sliding distance of silica sand and ferrochrome slag components to the mix, indicating improved wear resistance. The slag-furnace constituent, however, exhibits an opposite trend: COF increases with the sliding range. It is interesting to note that the COF of the ferrochrome slag samples increases steeply at the beginning, then gradually decreases over a short distance before sharply reducing at both velocities. As the slide continues, COF becomes more widely distributed, possibly due to changes in the surface conditions. Changes in the COF curves of blast furnace slag and silica sand occur more gradually than they occur abruptly. Although there are no significant differences in the blast furnace slag, and the COF does not vary significantly, the silica in the silico sand silica exhibits minimal variations, provided the distance of sliding is taken into account. The heat generated during wear resistance-enhancing heat treatment, which promotes grain refinement, reduces the COF of silica sand and ferrochrome slag components. Meanwhile, the increased hardness of blast furnace slag is also associated with increased COF, which offsets surface wear at long distances under sliding and results in variation in COF values. Unlike the overall trend, an increase in hardness reduces COF as plastic deformation is restricted. Thus, the sliding is smoother, the BFS sample had an even smaller initial COF, even though it was less hard. This anomaly is attributed to the formation of a thin oxide layer and favourable starting contact conditions in BFS castings, which temporarily reduced the friction but only in the initial sliding cycles. However, the COF values increased with constant loading as the oxide layer disintegrated [24]. Therefore, tribological behaviour is governed by the combination of hardness, surface film stability, and sliding duration. Moreover, surface integrity and microstructural features play a significant role; low COF is typically the consequence of coarse grains and enhanced wear resistance. The COF behaviour reflects the combined influence of hardness, grain structure, and dominant wear mechanisms. Due to the coarseness of the contact surface, ferrochrome slag castings initially exhibited high COF. Nevertheless, the tribo-layer appeared after some time of sliding, reducing variations and stabilising friction. Throughout testing, silica sand specimens demonstrated a moderate COF due to their balanced hardness and grain refinement. Blast furnace slag castings, on the other hand, showed higher COF, which was associated with coarser grains and more surface asperities that encouraged adhesion and micro-abrasion. Overall, the findings show that by promoting surface passivation, stabilising wear mechanisms, and reducing COF during repeated sliding, finer microstructures improve long-term tribological performance.

The COF trends demonstrate the dynamic evolution of surface films and contact mechanics during sliding. The formation of protective tribo-layers caused ferrochrome slag castings to stabilise after initially exhibiting increased friction due to asperity contact. Because of its uniform wear tracks and balanced hardness, silica sand maintained a moderate level of friction. Because of the formation of unstable oxide films and the exposure of coarser grains, blast furnace slag showed fluctuating COF. These behaviours demonstrate that surface chemistry, oxide stability, and grain morphology all affect tribological performance in addition to hardness. A longer component service life and enhanced wear resistance are indicated by lower, more stable COF values.

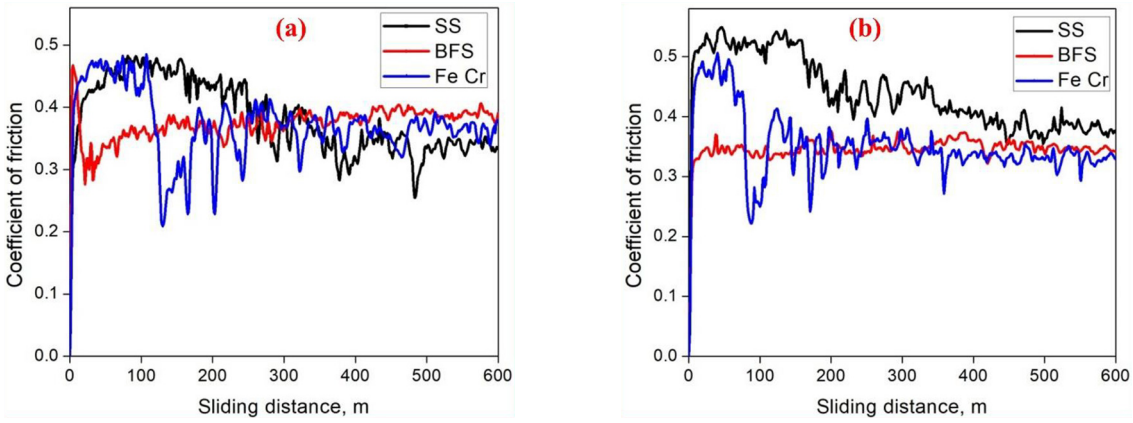

Figure 12. Coefficient of friction graph of a flat plate: (a) 600 rpm, (b) 780 rpm

Mass loss graph

Figure 13 illustrates the impact of rotational speed (600 rpm and 780 rpm) and a sliding distance of 600 meters on the wear-induced mass loss of AA2024 components cast using three different moulding sands. The findings show that, in both speed scenarios, wear mass loss steadily rises with sliding distance. At both rotational speeds, silica sand components showed the greatest mass loss of any mould. Blast furnace slag showed the lowest at 780 rpm, while ferrochrome slag showed the lowest at 600 rpm. A higher rotational speed (780 rpm) resulted in less mass loss than 600 rpm, which was unexpected. This unexpected trend is explained by strain hardening, which occurs due to the extreme stress of the component from increased frictional contact with the disc. The increased stress at higher speeds strengthens the resistance of AA2024 to material removal, as it is a strain-hardening alloy, thereby reducing wear loss. While blast furnace slag benefited from increased strain hardening at 780 rpm, the superior mechanical and thermal qualities of ferrochrome slag likely contributed to its minimal wear mass loss at 600 rpm. Nevertheless, the wear behaviour of silica sand components showed a sharp increase in mass loss at both speeds, indicating lower wear resistance [9]. Ferrochrome slag and blast furnace slag components, on the other hand, showed a slower, more controlled increase in mass loss, indicating more consistent wear behaviour over a range of distances and speeds. Reduced mass loss is not always ensured by higher hardness. Increased hardness in FCS castings was accompanied by brittle intermetallic phase fracture and unstable oxide films, which accelerated wear and material removal. BFS castings, on the other hand, exhibited better wear resistance, despite being relatively softer, due to the formation of stable oxide layers and smoother wear tracks, which reduced mass loss. These findings suggest that the stability of the oxide film, microstructural integrity, and the dominant wear mechanisms all contribute to controlling wear resistance, rather than hardness alone [25,26].

Mass loss analysis confirms that both mould type and sliding speed strongly influence wear resistance. Ferrochrome slag castings exhibited the least wear at 600 rpm, due to their stable surface integrity and refined grain structure. Due to improved strain-hardening, blast furnace slag castings exhibited less mass loss under higher stress conditions at 780 rpm. On the other hand, silica sand castings were consistently the most worn due to their lower hardness and coarser grains. These findings unequivocally demonstrate that both the current tribological conditions and microstructural features significantly influence the wear response of AA2024 castings.

Mass loss behaviour underscores the combined effects of microstructure and sliding velocity. Because stable oxide layers and refined grains shielded the contact surface, ferrochrome slag castings displayed minor wear at lower speeds. Because strain hardening increased abrasion resistance, blast furnace slag performed better at higher speeds [27]. Because silica sand samples had higher porosity and weaker tribo-layer formation, they consistently lost more mass. The unexpected decrease in wear at high speed emphasises the roles of plastic flow and thermal softening, which temporarily reduce abrasive interaction and stabilise the sliding interface.

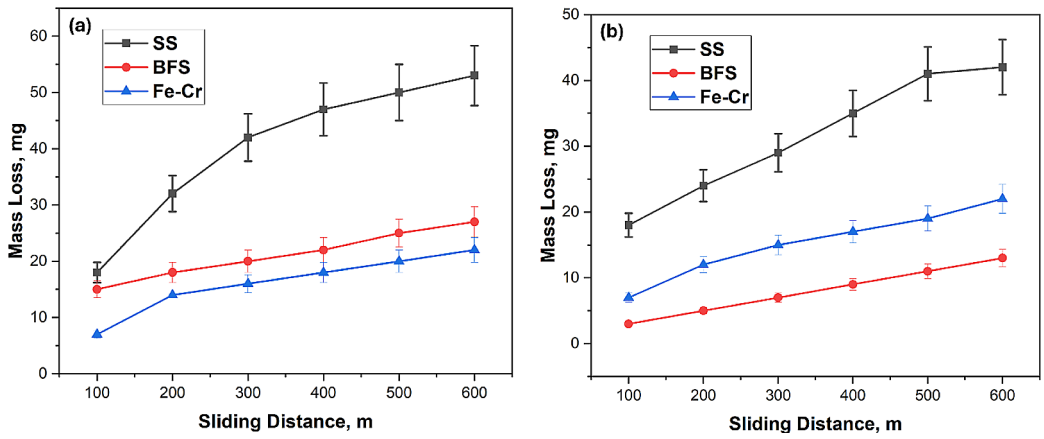

Figure 13. Mass loss graph for flat plate – sliding distance: (a) 600 rpm (b) 780 rpm

Wear rate analysis

Figures 14a and 14b clearly show that at the two rotating speeds, 680 rpm and 780 rpm, the moulded silica sand components have the highest wear rate among all the samples. Conversely, the blast furnace slag at 780 rpm and the ferrochrome slag at 600 rpm wear out the least. What is interesting to observe in this case is that the general rule that the wear rate increases with rotational speed is not followed. Instead, wear rates rise as the speed is reduced. This anomaly is attributed to increased heat production and friction at higher speeds, which softens the contact surface, diminishes wear through localised plastic deformation, and provides a lubricating effect. All kinds of moulds tend to wear out as the sliding distance increases. The wear rate would initially increase, then either level off or decrease with further sliding, after approximately 100 meters. This trend would mean that the contact surface could stabilise, allowing the material to transfer as the component continues to slide, thereby reducing material movement. The wear rate profiles exhibit slight oscillation, featuring both soft and hard linear and nonlinear wear patterns. These variations can be explained by dynamic changes in contact pressure and material softening over time, which intermittently alter the frictional behaviour [28]. It is observed that whereas other parts exhibit a more linear reduction in wear rate, silica sand castings exhibit a very sharp reduction at the specified speeds [8]. This highlights the stabilising characteristics of slag-based moulds and the low wear resistance of silica sand. Also, this paper revealed that hardness and delamination-controlled wear are interrelated and complex. Although FCS-moulded samples were harder, wear and delamination were more prevalent due to brittle intermetallic phases and poor oxide film stability, which facilitated the initiation and propagation of cracks. BFS-moulded samples; however, had more stable oxide layers and smoother sliding surfaces that reduced wear and delamination, although they were relatively soft. Consequently, wear performance is governed by the product of hardness, oxide film stability, and general microstructural integrity, rather than hardness alone [29].

Wear rate analysis revealed that silica sand castings exhibited the most significant material removal, primarily due to their low hardness and poor microstructural stability. On the other hand, ferrochrome slag castings exhibited higher wear resistance at lower speeds, with less material loss due to increased hardness and finer grains. Slag castings in blast furnaces worked better in high sliding speeds due to strain hardening, which reduced surface damage and enhanced resistance. Additionally, the wear rate has been observed to decrease with increasing sliding distance, indicating the formation of protective tribo-layers and the influence of thermal softening, which stabilises wear processes over time. In general, these data indicate that selecting the appropriate moulding material is critical to the long-term performance of AA2024 castings in sliding wear.

In Figures 15 and 16, SEM images of the worn surfaces of AA2024 components cast in moulds made from silica sand, blast furnace slag, and ferrochrome slag at two rotational speeds, 600 rpm and 780 rpm, are provided. The photographs show rough, sticking wear patterns in all the samples. The wear debris from each component suggests distinct abrasive wear, probably

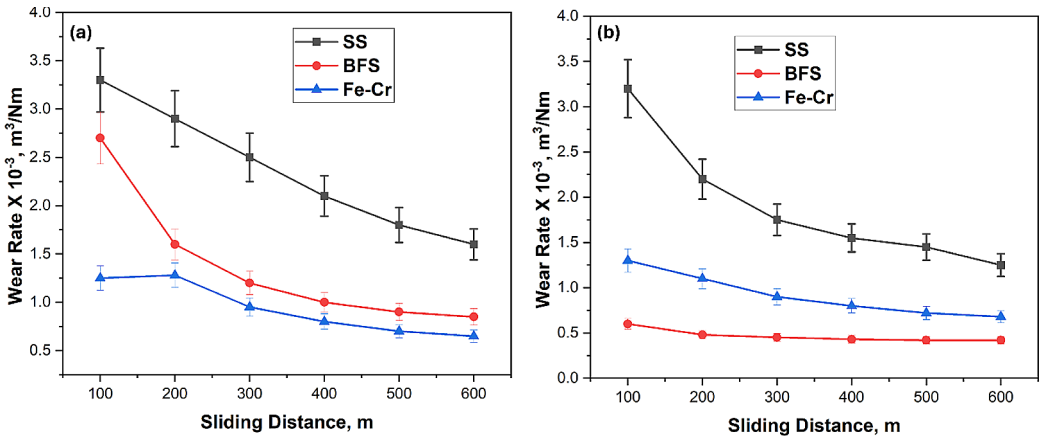

Figure 14. Wear rate graph: a) 600 rpm, b) 780 rpm

followed by oxide, which extends along the wear tracks and forms debris.

The silica sand sample has definite surface scratching at 600 rpm. However, as shown in Figure 15c, the ferrochrome slag specimen exhibits fewer scratches and appears to have undergone severe plastic deformation, characteristic of ploughing, smearing, and cutting. Trapped, plastically deformed debris also indicates intense surface interaction. The same phenomenon repeats at 780 rpm; however, scratching is less evident, and plastic deformation is more pronounced than at 600 rpm, suggesting that higher temperatures may increase the softness of the material and reduce direct abrasion [30]. The same response is supported by Figures 16(a–c), which have fewer surface scratches than Figure 15(a–c) does. Three-body abrasive wear is characterised by material removal in patches, particularly around loose particles, which in turn cause further abrasion. Compared to the condition at 600 rpm, all three components exhibit reduced abrasive wear and reduced debris generation at high speed. Additionally, delamination wear is observed, likely due to poor work hardening in certain areas, which causes them to separate into softer regions. The more pronounced grooves in Figures 16b–16c and 15b–15c) indicate elevated contact temperatures, leading to surface softening and increased abrasive effects. All in all, the most prevalent at both speeds is abrasion, with its severity decreasing as rotational speed increases due to thermal softening.

Wear rate results further validate that tribological performance is governed by microstructural stability rather than hardness alone. At moderate speeds, ferrochrome slag castings showed superior resistance due to their refined grain structure, which prevented delamination. Deformation-induced strain hardening at high speeds reduced material removal in blast furnace slag. Because coarse grains and unstable oxide films made it easier for cracks to start and debris to form, silica sand samples showed higher wear rates. The development of protective tribo-layers and surface smoothing is indicated by the progressive decrease in wear rate with increasing sliding distance, highlighting the significance of maintained microstructural integrity in long-term wear applications.

The use of ferrochrome slag in moulding applications may be subject to regulatory and environmental scrutiny due to possible heavy-metal leaching and waste classification

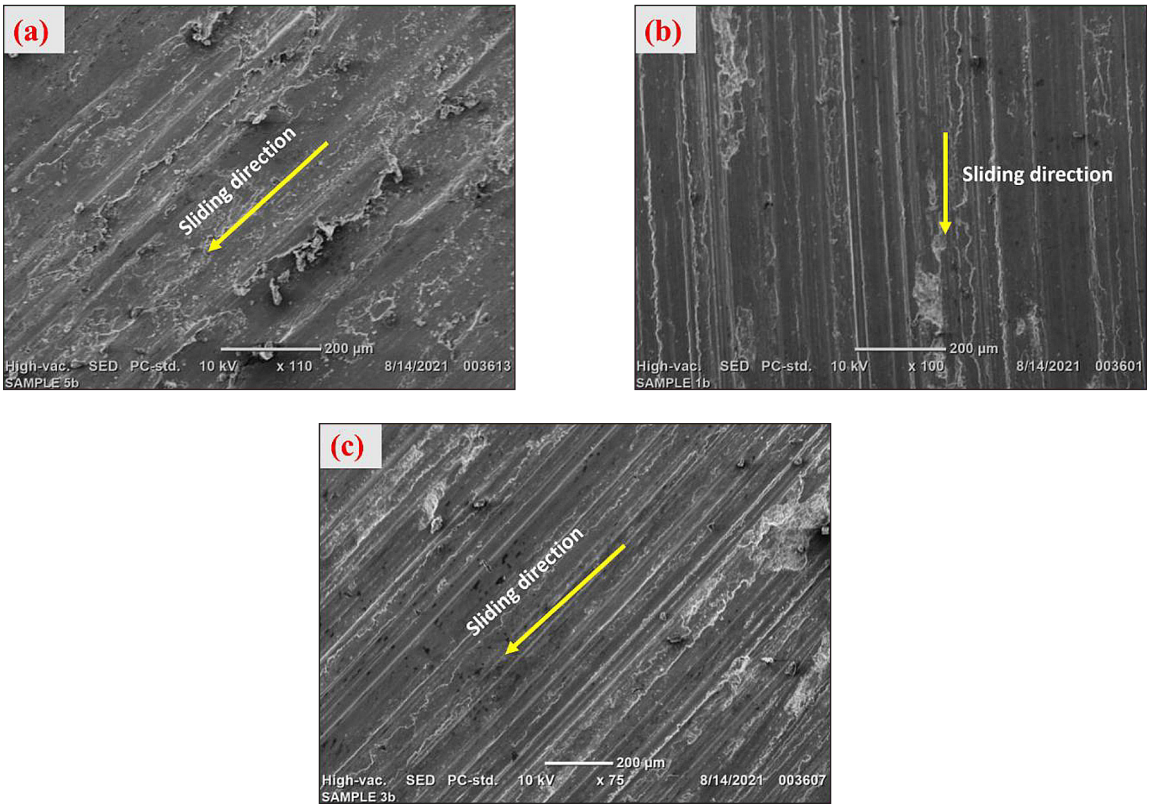

Figure 15. Wear morphology at 600 rpm: (a) silica sand, (b) blast furnace slag, (c) ferrochrome slag

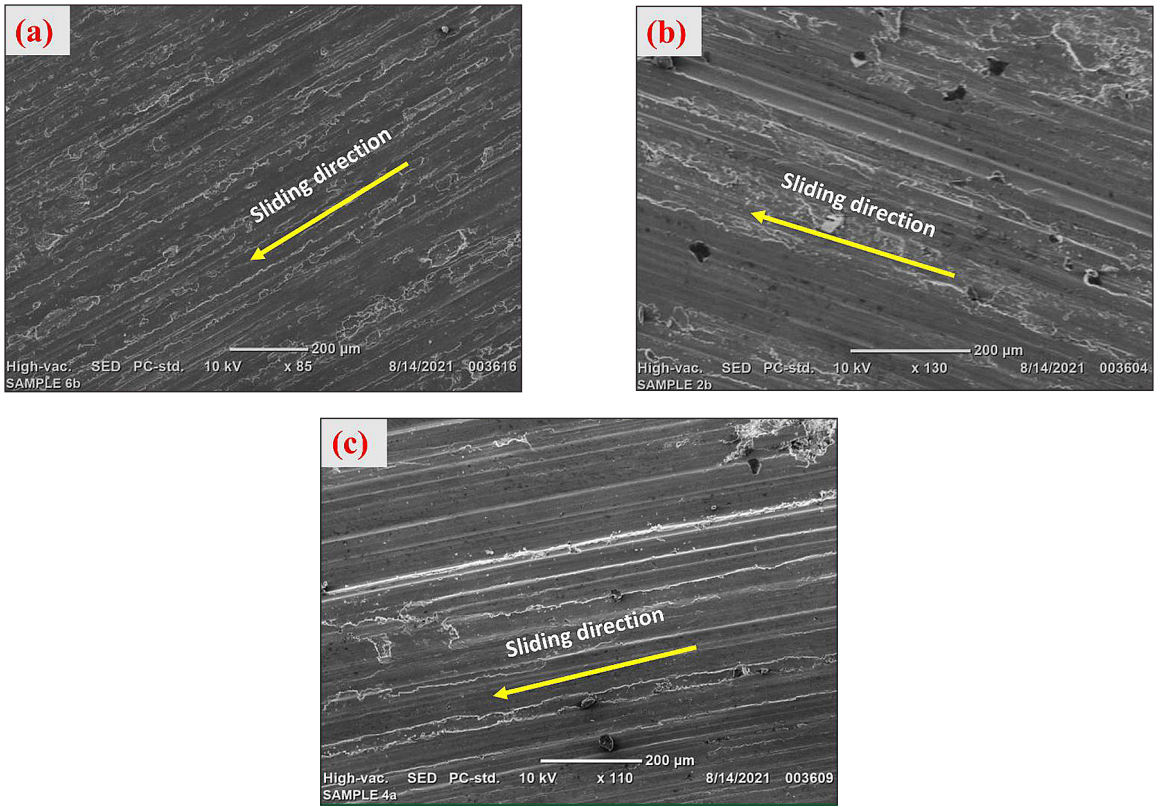

Figure 16. Wear morphology at 780 rpm: (a) silica sand, (b) blast furnace slag, (c) ferrochrome slag

guidelines. Nonetheless, earlier research shows that encapsulation in mould binders, controlled processing, and particle stabilisation considerably lowers environmental risk. Before industrial adoption, routine leachability testing and adherence to national pollution control standards are advised. Ferrochrome slag can be used as a sustainable, safe substitute for mould material when appropriately treated and certified.

CONCLUSIONS

Ferrochrome slag moulds had the highest density (~2.74 g/cm³), comparable to the theoretical density of AA2024 (2.78 g/cm³), and showed negligible microporosity. Blast furnace slag had a density of around 2.71 g/cm³, while silica sand had the lowest density (around 2.68 g/cm³) – higher density connected with faster cooling and better internal soundness. Although statistically significant, the findings are based on a small sample size; thus, larger casting batches are required for industrial validation. Ferrochrome slag had the smallest grain size (~75 ± 2 µm), followed by silica sand (~101 ± 3 µm) and blast furnace slag (~115 ± 5 µm). Reduced secondary dendritic arm spacing increased strength and wear resistance via Hall-Petch strengthening. While optical microscopy demonstrated consistent refinement, advanced EBSD validation was not performed, resulting in minimal ambiguity. Nonetheless, the evident particle size hierarchy demonstrates the thermal advantage of slag-based moulds.

Thermal profiling found that ferrochrome slag had the steepest cooling gradient, lowering the centre temperature more quickly during the first 10–15 minutes than silica sand and blast furnace slag. A higher estimated thermal diffusivity favoured refined grains and reduced porosity. However, the computations used literature thermophysical values rather than actual measurements, which may have included some estimation error. Future direct conductivity testing would increase predicted accuracy.

Ferrochrome slag castings had the highest microhardness (~153.5 HV), surpassing silica sand (~139 HV) and blast furnace slag (~134.5 HV). Finer grains and lesser porosity are responsible for the 10-15% increase in hardness. Local hardness discrepancies represented unequal mould cooling. Although statistically validated, nano-scale precipitate analysis was not undertaken; hence, micro-phase strengthening

mechanisms are only partially inferred, rather than experimentally confirmed.

Silica sand castings had somewhat higher tensile strength (about 3–5% increase) due to balanced cooling, while ferrochrome slag supplied equivalent strength with fewer internal flaws. Blast furnace slag had lower tensile values because microporosity served as a stress concentrator. The strength-ductility trade-off was clear. However, no long-term fatigue or corrosion-assisted tensile testing was performed, limiting the capacity to forecast lifecycle mechanical reliability.

Blast furnace slag moulds had the best compressive strength (about 8–12% higher than others) due to improved strain hardening despite finer grains. Ferrochrome slag exhibited lower compressive resistance but higher hardness. Silica sand remained intermediate. These data suggest that compressive performance is more dependent on plastic deformation than grain refinement. Cyclic compression and thermal stress testing were not conducted, resulting in uncertainty in long-term load-bearing predictions.

Silica sand had the lowest surface roughness values (~0.415 Ra), followed by ferrochrome slag (~0.458 Ra) and blast furnace slag (~0.463 Ra). Slag moulds with a roughness increase of ~10% showed increased hardness and chip instability during machining. Although the surface smoothness decreased marginally, the mechanical benefits remained excellent. Fixed machining parameters may have influenced the results, and adaptive cutting optimisation could further reduce roughness.

Ferrochrome slag initially had a higher COF (~1.25 at 100 m), but stabilized to ~0.65 at 600 m due to tribo-layer development. Blast furnace slag fluctuated between 0.6 and 1.2 due to oxide instability, while silica sand remained stable at around 0.9-1.6. These trends emphasise the importance of grain refining and surface chemistry. Lubricated and high-temperature circumstances were not investigated, which limits direct real-world tribological extrapolation.

At 600 rpm, ferrochrome slag lost the least mass (~21 mg at 600 m), followed by blast furnace slag at 780 rpm (~13 mg), while silica sand lost the most (~53 mg at 600 m). Reduced porosity and polished grains improved wear resistance. Despite substantial statistical differences, no long-duration cyclic wear or corrosion-abrasion tests were conducted, limiting the accuracy of extended-service-life predictions.

The wear rate decreased with sliding distance, with ferrochrome slag showing the best resistance (~0.65 × 10^{-3} $mm^3/N \cdot m$ at 600 m), blast furnace slag performing better at higher speeds (~0.42 × 10^{-3} $mm^3/N \cdot m$), and silica sand exhibiting the highest wear. The creation of a protective tribo-layer increased the stability. Although the trends are considerable, the lack of long-cycle environmental wear testing prevents long-term durability validation.

Although the present investigation primarily focused on immediate mechanical and tribological behaviour, the observed microstructural refinement, reduced porosity, and stable oxide film formation in ferrochrome slag castings suggest favourable long-term performance compared with conventional silica sand moulds. Increased hardness and wear resistance imply improved durability under frequent sliding and load-bearing conditions. However, this work lacked thorough long-term validation methods, such as thermal ageing analysis, corrosion exposure studies, and cyclic fatigue testing. Therefore, to establish definitive long-term performance equivalency, future studies are advised to conduct extended lifecycle and environmental stability assessments, even though preliminary indicators are encouraging.

The present study has certain limitations that should be acknowledged. A small number of samples were used in the laboratory-scale castings used for the experimental investigations, which could have introduced variability in the measured properties. Aspects of long-term performance, such as oxidation behaviour, corrosion resistance, thermal fatigue, and cyclic loading, were inferred from the literature and microstructural indicators rather than experimentally assessed. Additionally, repeatability may be impacted by slight variations in slag chemistry and morphology, despite efforts to guarantee uniform particle size and binder ratio. Only primary mechanical and tribological properties were subject to statistical analysis. To fully confirm industrial applicability, future research should include extensive durability testing, comprehensive environmental evaluations, and large-scale casting trials.

Acknowledgements

The authors would like to express their gratitude to the Symbiosis International University for the funding arrangements.

REFERENCES

1. Murthy IN, Babu NA, Rao JB. Microstructure and mechanical properties of A356 alloy castings made in sand and granulated blast furnace slag moulds. Mater Today Proc 2018;5:161–7.
2. Acharya PK, Patro SK. Use of ferrochrome ash (FCA) and lime dust in concrete preparation. J Clean Prod 2016;131:237–46.
3. Idris J, Al-Bakoosh A. Application of non-destructive testing techniques for the assessment of casting of AA5083 alloy. Journal of Advanced Research in Applied Mechanics 2014;3:25–34.
4. Murthy IN, Rao JB. Non destructive evaluation of A356 alloy castings made in sand and granulated blast furnace slag moulds. Mater Today Proc 2018;5:168–74.
5. Murthy IN, Rao JB. Investigations on physical and chemical properties of high silica sand, Fe-Cr slag and blast furnace slag for foundry applications. Procedia Environ Sci 2016;35:583–96.
6. Karthick S, Siddharth CSK, LV KA, Thenarasu M. Evaluation of mechanical properties economic and environmental benefits of partially replacing silica sand with biomass ash for aluminium casting. Mater Today Proc 2018;5:12984–92.
7. Tijani Y, Heinrietz A, Bruder T, Hanselka H. Quantitative evaluation of fatigue life of cast aluminum alloys by non-destructive testing and parameter model. Int J Fatigue 2013;57:73–8.
8. Bejaxhin ABH, Paulraj G, Prabhakar M. Inspection of casting defects and grain boundary strengthening on stressed Al6061 specimen by NDT method and SEM micrographs. Journal of Materials Research and Technology 2019;8:2674–84.
9. Patil SA, Darade PD. Application and performance frequency response method as NDT tool to detect defects in castings. Mater Today Proc 2017;4:8463–8.
10. Khan MWA, Ahmad R, Bukhari SMA, Sultan M, Husnain N, Anwar MT, et al. Influence of vibration-assisted dynamic solidification on microstructure and mechanical properties of permanent Mold cast aluminum alloy 2024 with conformal cooling. Journal of Manufacturing and Materials Processing 2025;9:416.
11. Wang R, Zhu Q, Zuo Y, Cheng L, Wang J. The control of as-cast structure of 2024 aluminum alloy with intensive melt shearing and its effect on microstructure and mechanical properties after T4 treatment. Journal of Materials Research and Technology-JMR&T 2023;24:3179–93.
12. Rafi SM, Satish Kumar T, Thankachan T, Selvan CP. Synergistic effect of FSP and TiB_2 on mechanical and tribological behavior of AA2024 surface composites. J Tribol 2023;145.
13. Li X, Zhang L, Li Y, Zhao Y, Guo Z, Wang H, et al. Advances in additive manufacturing of cemented carbides: from powder production to mechanical properties and future challenges. Curr Opin Solid State Mater Sci 2025;38:101238.
14. Ramesh CS, Keshavamurthy R. Influence of forging on mechanical properties of Ni–P coated Si3N4 reinforced Al6061 composites. Materials Science and Engineering: A 2012;551:59–66.
15. Guo P, Xue R, Zou Q, Ma X, Su C, Zeng Z, et al. Enhanced ultramicropore of biomass-derived porous carbon for efficient and low-energy CO_2 capture: Integration of adsorption and solar desorption. Energy & Environmental Materials 2025:e70140.
16. Kavya JT, Keshavamurthy R, Kumar GSP. Studies on parametric optimization for abrasive water jet machining of Al7075-TiB2 in-situ composite. IOP Conf. Ser. Mater. Sci. Eng., 149, IOP Publishing; 2016, 012024.
17. Satyanarayana MVNV, Kumar A. Microstructure evolution, mechanical, and corrosion behavior of cryogenic friction stir-processed AA2014 alloy. Adv Eng Mater 2021;23. https://doi.org/10.1002/adem.202100301
18. Keerthana BVS, Satyanarayana MVN V, Reddy KV, Shankar MNR. Microstructure, mechanical characteristics, and electrochemical behavior of the wide-area stir zone fabricated in Al5083 by friction stir processing with overlapping technique. Proc Inst Mech Eng C J Mech Eng Sci 2024;238:505–14.
19. Keshavamurthy R, Arunachalam KP, Kumar MA, Chiranjeevi P, Reddy RS, Chekuri RBR, et al. Microstructural evolution and damping response in ARB-processed ZK60 alloy. Canadian Metallurgical Quarterly 2025:1–13.
20. Immarigeon JP, Holt RT, Koul AK, Zhao L, Wallace W, Beddoes JC. Lightweight materials for aircraft applications. Mater Charact 1995;35:41–67.
21. Satyanarayana M, Bathula S, Kumar A. Effect of external cooling on fatigue crack growth behaviour of friction stir processed AA6061 alloy. Eng Fract Mech 2022;261:108236.
22. Kumar PH, Srivastava A, Kumar V, Majhi MR, Singh VK. Implementation of industrial waste ferrochrome slag in conventional and low cement castables: Effect of microsilica addition. Journal of Asian Ceramic Societies 2014;2:169–75.
23. Bejaxhin ABH, Paulraj G, Prabhakar M. Inspection of casting defects and grain boundary strengthening on stressed Al6061 specimen by NDT method and SEM micrographs. Journal of Materials Research and Technology 2019;8:2674–84.
24. Naveena BE, Keshavamurthy R, Sekhar N. Dry sliding wear behaviour of plasma sprayed Flyash-Al2O3

and Flyash-SiC coatings on the Al6061 aluminum alloy. Silicon 2019;11:1575–84.

25. Mehta KM, Badheka VJ. Wear behavior of boron-carbide reinforced aluminum surface composites fabricated by Friction Stir Processing. Wear 2019;426–427:975–80. https://doi.org/10.1016/j.wear.2019.01.041.
26. Lal DM, Renganarayanan S, Kalanidhi A. Cryogenic treatment to augment wear resistance of tool and die steels. n.d.
27. Pradeep Kumar GS, Keshavamurthy R, kuppahalli P, kumari P. Influence of Hot forging on Tribological behavior of Al6061-TiB2 In-situ composites. IOP Conf. Ser. Mater. Sci. Eng., 149, IOP Publishing; 2016, 012087.
28. Vijayakrishna B, Mrudula G, Sagar Y, Prakash P, Janaki DV, Satyanarayana M. Mechanical properties enhancement in friction stir processed AA2024 alloy through pin profile optimization. Journal of The Institution of Engineers (India): Series D 2025;106:1221–33.
29. Satyanarayana MVN V, Suresh BV, Janaki DV, Kumar A. Effect of overlapping technique on the grain size distribution and grain orientation in friction stir processed aluminum alloys. Proceedings of the Institution of Mechanical Engineers, Part L: Journal of Materials: Design and Applications 2024;238:198–203.
30. Reddy V, Rambabu V, Mrudula G, Prakash P, Venkatesh DJ, Mudunuri R, et al. Effect of shot peening on microstructural features, residual stress behavior, and hardness of aluminum alloy 2014. Engineering Research Express 2025;7:015527.